Earth and Planetary Science Letters 401 (2014) 70–82

Contents lists available at ScienceDirect

Earth and Planetary Science Letters

www.elsevier.com/locate/epsl

Impact of dissolution on the sedimentary record of the Paleocene–Eocene thermal maximum

Timothy J. Bralower [a,b,*], D. Clay Kelly [c], Samantha Gibbs [d], Kenneth Farley [e], Laurie Eccles [a], T. Logan Lindemann [a], Gregory J. Smith [a]

[a] Department of Geosciences, Pennsylvania State University, University Park, PA 16802, USA
[b] Climate Change Research Centre, University of New South Wales, Sydney, 2052, Australia
[c] Department of Geoscience, University of Wisconsin, Madison, WI 53706, USA
[d] Ocean and Earth Science, National Oceanography Centre, Southampton, University of Southampton, Southampton, SO14 3ZH, UK
[e] Division of Geological and Planetary Sciences, California Institute of Technology, Pasadena, CA 91125, USA

ARTICLE INFO

Article history:
Received 23 October 2013
Received in revised form 10 May 2014
Accepted 27 May 2014
Available online xxxx
Editor: G.M. Henderson

Keywords:
dissolution
chemical erosion
nannofossils
planktonic foraminifera
Paleocene Eocene thermal maximum

ABSTRACT

The input of massive amounts of carbon to the atmosphere and ocean at the Paleocene–Eocene Thermal Maximum (PETM; ~55.53 Ma) resulted in pervasive carbonate dissolution at the seafloor. At many sites this dissolution also penetrated into the underlying sediment column. The magnitude of dissolution at and below the seafloor, a process known as chemical erosion, and its effect on the stratigraphy of the PETM, are notoriously difficult to constrain. Here, we illuminate the impact of dissolution by analyzing the complete spectrum of sedimentological grain sizes across the PETM at three deep-sea sites characterized by a range of bottom water dissolution intensity. We show that the grain size spectrum provides a measure of the sediment fraction lost during dissolution. We compare these data with dissolution and other proxy records, electron micrograph observations of samples and lithology. The complete data set indicates that the two sites with slower carbonate accumulation, and less active bioturbation, are characterized by significant chemical erosion. At the third site, higher carbonate accumulation rates, more active bioturbation, and possibly winnowing have limited the impacts of dissolution. However, grain size data suggest that bioturbation and winnowing were not sufficiently intense to diminish the fidelity of isotopic and microfossil assemblage records.

1. Introduction

Unabated anthropogenic carbon emission looms as an increasingly significant threat to the ocean and its inhabitants. It has been estimated that the ocean has absorbed roughly a third of the carbon emitted, which is causing a decrease in carbonate ion content and pH (e.g., Broecker and Takahashi, 1977; Caldeira and Wickett, 2005), a response known as ocean acidification (e.g., Feely et al., 2004; Orr et al., 2005; Doney et al., 2009). However, the long-term impact of increased CO_2 emission on the marine carbon cycle is not clear, nor is it resolved how the system will respond once emission levels decrease. Acidification poses a substantial threat to organisms that form shells of the minerals aragonite and calcite and plays an important role in carbon drawdown. Thus intensive investigations of the modern ocean, its biogeochemical cycles and ecosystems are underway (e.g., Kleypas and Yates, 2009; Beaufort et al., 2011; Pandolfi et al., 2011; Lohbeck et al., 2012).

Ancient abrupt warming events, such as the Paleocene–Eocene thermal maximum (PETM; ~55.53 million years before present; Westerhold et al., 2008), provide an opportunity to constrain the impact of massive carbon input on the oceans and their ecosystems over millennial time scales (e.g., Dickens et al., 1997; Zeebe and Zachos, 2007). Consequently, marine environments, chemical cycles, and the fossil record of the PETM have been studied in detail (e.g., Thomas and Shackleton, 1996; Thomas et al., 2002; Wing et al., 2005; Zachos et al., 2005, 2007; Sluijs et al., 2007a, 2007b; Foster et al., 2013; Zeebe and Zachos, 2013; Penman et al., 2014).

The onset of the PETM involved the introduction of vast quantities of carbon to the ocean–atmosphere system as signified by the abrupt ~3–4‰ carbon isotope excursion (CIE) at the base of the event. Estimates for the mass and rate of carbon input vary substantially, ranging from ~2000 Pg to as high as 6800 Pg over approximately 1 kyr to 50 kyr (Dickens et al., 1995; Panchuk et al., 2008; Zeebe et al., 2009; Cui et al., 2011; Dickens, 2011;

* Corresponding author. Tel.: +1 814 863 1240.
E-mail address: bralower@psu.edu (T.J. Bralower).

http://dx.doi.org/10.1016/j.epsl.2014.05.055
0012-821X/

Sluijs and Dickens, 2012). The greenhouse effect of the carbon addition, in conjunction with positive feedback mechanisms, was sufficient to induce warming of ocean surface and deep waters by 6–8 °C (e.g., Zachos et al., 2001, 2003; Zeebe et al., 2009), increase stratification in some locations, and likely alter ocean circulation patterns (e.g., Thomas et al., 2003; Nunes and Norris, 2006; Zeebe and Zachos, 2007; Lunt et al., 2010). The combined effects of warming and changing circulation conspired to lower oxygen levels and alter patterns of primary productivity, thereby modifying habitats from the surface ocean (e.g., Kelly et al., 1998; Crouch et al., 2001; Bralower, 2002; Kelly, 2002; Gibbs et al., 2006a; Agnini et al., 2007; Sluijs et al., 2007a; Raffi et al., 2009; Nicolo et al., 2010; Winguth et al., 2012; Norris et al., 2013) down to its depths where the PETM corresponds to the largest extinction of deep sea benthic foraminifera in the last 93 million years (e.g., Thomas, 1990, 1998, 2003, 2007).

Many of the expected changes in carbon cycling predicted for the future occurred during the PETM (e.g., Ridgwell and Schmidt, 2010; Hönisch et al., 2012; Zeebe and Zachos, 2013). The base of deep-sea PETM records show an abrupt decrease in $CaCO_3$ content, a deterioration in microfossil preservation, a sharp drop in sedimentation rate, and a discrete claystone layer (e.g., Thomas, 1998; Zachos et al., 2005; Bralower et al., 2006; Colosimo et al., 2006). These changes indicate major decreases in the carbonate saturation of intermediate- and deep-ocean waters leading to substantial shoaling of two key surfaces: the lysocline, which is the level at which the rate of dissolution of carbonate particles sinking through the water column increases (e.g., Berger and Winterer, 1974), and the calcite compensation depth (CCD), which is the depth at which all of the settling calcite is removed via dissolution (Zachos et al., 2005).

Corrosive PETM bottom waters dissolve carbonate particles settling to the sea floor as well as those in the actively burrowed uppermost 10 cm of the sediment column (e.g. Walker and Kasting, 1992; Archer et al., 1997, 1998; Dickens et al., 1997; Dickens, 2000). In cases where all of the carbonate is removed in the bioturbated zone, dissolution had the potential to remove previously deposited carbonate layers (Zachos et al., 2005; Colosimo et al., 2006; Kelly et al., 2010, 2012). Terminology for these processes varies between authors; hence to accurately represent the location of dissolution, we use the term *syn-depositional dissolution* for dissolution of newly deposited carbonate in the bioturbated benthic transition layer to distinguish it from *burndown dissolution*—which refers to dissolution of previously deposited layers below this interval. We use the term *chemical erosion* to refer collectively to syn-depositional and burndown dissolution.

Understanding chemical erosion is critical because of its potential to remove key stratigraphic horizons from the onset of PETM records and the interval immediately proceeding it. However, because dissolution removes carbonate materials, it is a notoriously difficult process to detect in the sedimentary record. For this reason, much of our understanding of chemical erosion derives from geochemical models designed to simulate the response of the marine carbonate system to carbon input (e.g., Dickens et al., 1997; Ridgwell, 2007; Ridgwell and Hargreaves, 2007; Zeebe and Zachos, 2007; Panchuk et al., 2008). Because the onset of the PETM occurs over centimeters in deep-sea sediment records, chemical erosion is recognized as complicating the interpretation of the stratigraphy of the earliest stages of the event (e.g., Murphy et al., 2010), but how it has obscured isotopic and other proxy records has not been determined. Without this information, the magnitude of environmental changes can only be estimated with any accuracy in sections from above the lysocline, most of which lie on continental shelves. Still, the PETM represents a great opportunity to understand the impact of dissolution on the stratigraphic record because of the existence of numerous calcareous sections arrayed over a broad range of ocean depths, including depth transects (e.g., Zachos et al., 2005; Bralower et al., 2006).

Foraminiferal fragmentation is generally considered the most reliable indicator of dissolution in deep-sea sediments (e.g., Arrhenius, 1952; Thunell, 1976; Haug and Tiedemann, 1998; Le and Shackleton, 1992; Howard and Prell, 1994; Hancock and Dickens, 2006). Dissolution during the PETM indeed led to an increase in fragmentation, the proportion of foraminiferal shells that are fragments or broken (e.g., Kelly et al., 2005, 2010; Colosimo et al., 2006), and complete dissolution of carbonate at sites below the CCD produced fragmentation levels approaching infinity (e.g., Kelly et al., 2010; Leon-Rodriguez and Dickens, 2010). Considerably less is known about the effect of dissolution on nannoplankton, the dominant component of many deep-sea sediments, including those that record the PETM. For reasons not fully understood, it is thought that the calcite crystal arrangement or the higher surface areas of some nannofossils tends to make them more resistant to dissolution than most planktic and calcareous benthic foraminifera (e.g., Schlanger and Douglas, 1974; Broecker and Clark, 1999; Chiu and Broecker, 2008). The PETM at all open-ocean sites corresponds to an increase in dissolution-resistant nannofossil species (Raffi and De Bernardi, 2008; Gibbs et al., 2010; Dedert et al., 2014), in part an ecological response to changes in surface environments. However, changes in the volumetric abundance of nannofossils in the PETM has never been determined largely because these fossils are roughly two orders of magnitude smaller than their foraminiferal counterparts, making them difficult to analyze with the same grain-size technique.

Because of their size, foraminifera and especially nannofossils are susceptible to redistribution by processes such as bioturbation (mixing by burrowing infauna) and winnowing through the resuspension of fine-grained material by bottom currents on the deep-sea floor (e.g., Stow et al., 2002). Thus both processes are a key part of interpreting data from high-resolution (cm-scale) PETM studies (e.g., Thomas, 2003; Stoll, 2005; Zachos et al., 2007). Also, models indicate that bioturbation impacts chemical erosion (e.g., Archer et al., 1997; Zeebe and Zachos, 2007; Panchuk et al., 2008), but this hypothesis has not been tested with data. Burrows are readily observed in sediments and their density and diversity provide a measure of the degree of bioturbation (e.g., Savrda et al., 1984). The occurrence of winnowing can be interpreted from grain size distributions (e.g., McCave et al., 1995; Kranck et al., 1996).

Here we focus on the impact of dissolution on nannoplankton and planktic foraminifera in sediments that record the PETM. We combine grain size analyses and electron microscopy of sediments from three sites that were affected to varying degrees by dissolution during the event. These data shed light on the mechanics of dissolution during the event, the identification of syn-depositional and burndown dissolution in PETM sections, and the impact of dissolution, bioturbation and winnowing on the stratigraphy of the event. Ultimately, this knowledge allows us to identify sections where the full suite of acidification responses can be investigated.

2. Material and methods

Sediment samples were obtained from across the PETM at Ocean Drilling Program (ODP) Site 1209 (Shatsky Rise, Central Pacific; 32°39.1′N, 158°30.4′E; 2387 m water depth; 1900 m paleodepth, Takeda and Kaiho, 2007), ODP Site 1262 (Walvis Ridge, South Atlantic; 27°11.2′S, 1°34.6′E; 4755 m water depth; 3600 m paleodepth, Zachos et al., 2005), and from the lower part of the PETM at ODP Site 690 (Maud Rise, Weddell Sea; 65°9.6′S, 1°12.3′E; 2925 m water depth; 1900–2000 m paleodepth, Thomas, 1990), (Fig. 1). At Site 690 the PETM corresponds to a ~2.5 m interval of cyclically alternating white to pale brown calcareous ooze (Fig. 2).

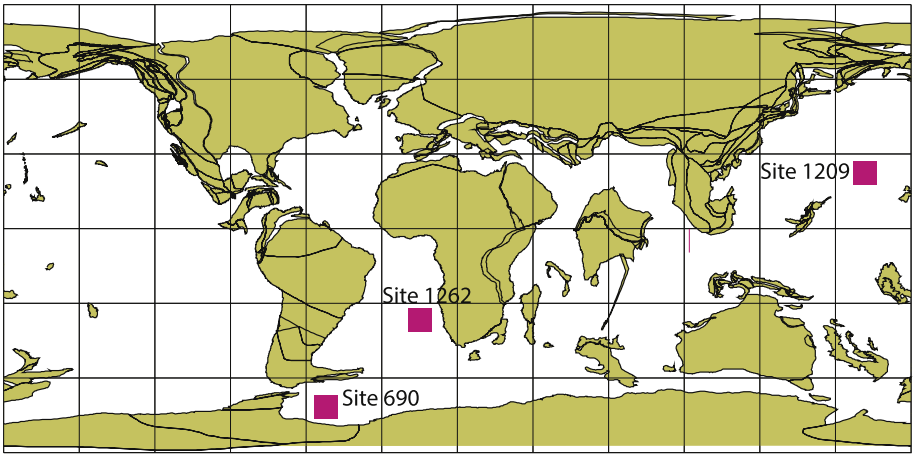

Fig. 1. Locations of the sites studied plotted on a 55 Ma paleogeography (www.odsn.de).

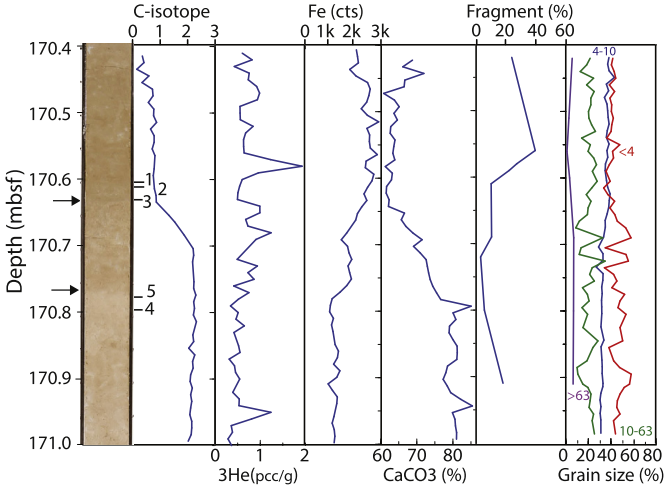

Fig. 2. Lithology, chemical and grain size data from the PETM at Site 690. Sediments are moderately heavily bioturbated throughout the study interval. Arrows refer to color changes discussed in text; 1-decline in fragmentation, 2-BFE, 3-CIE, 4-decrease in $CaCO_3$ content, 5-deterioration of nannofossil preservation (see text and Supplemental Materials Table 2). Fe content in thousand counts per second derived by XRF scanning from Röhl et al. (2000), maximum values is 3000 cps; Bulk carbonate isotope data from Thomas et al. (2002). $CaCO_3$ and fragmentation data derived from Kelly et al. (2005) and herein. ^{3}He data from Farley and Eltgroth (2003). Sediments above lowermost arrow impacted by syndepositional dissolution. (For interpretation of the references to color in this figure, the reader is referred to the web version of this article.)

At Site 1209 the event lies in a ~25-cm-thick layer of clayey nannofossil ooze with a sharp basal contact and a gradational upper contact with underlying and overlying chalk, respectively (Fig. 3). Finally, at Site 1262 the PETM correlates to a ~20 cm-thick red clay layer, which also has a sharp basal contact and a gradational upper contact with surrounding carbonate ooze (Fig. 4). Site 1262 represents the deepest site of the Walvis Ridge drilling transect and is characterized by the most dramatic and prolonged dissolution during the PETM at this location (Zachos et al., 2005; Kelly et al., 2010).

Small volumes (<0.5 cc) of each sample were disaggregated in water for several hours. The size distribution of samples was determined using a Malvern Mastersizer in the Materials Research Laboratory (MRL) at Pennsylvania State University. This instrument provides an optical measurement of *volume percent* particle size between 0.1 and 1000 μm with a precision of 0.5–1%. All data are archived at NGDC (http://www.ngdc.noaa.gov). Malvern analyses are rapid, allowing us to collect a very high-resolution grain size data set. The precision of the Malvern, however, is known to be lower than other grain size analyzers such as the Coulter Counter (CC) or Sedigraph (e.g., McCave et al., 2006) which are generally used for limited grain size ranges (e.g., Hovan and Rea, 1992). Replicate analyses using the Malvern and CC demonstrate a high degree of accuracy in the <38 μm fraction (see discussion in Bralower et al., 2010). However, the Malvern appears to underestimate the percentage of larger particles (>63 μm) (McCave et al., 2006). This likely reflects the significantly larger surface volume of the dominant nannofossil size fraction compared to the >63 μm fraction, but may also reflect a measurement bias resulting from the way samples are introduced into the Malvern instrument (Liz Hajek, pers. comm., 2013). For this reason, we do not interpret Malvern >63 μm data, and, instead, use the *weight percent* >63 μm data previously acquired by conventional sample washing/sieving practices (e.g., Kelly et al., 2005, 2010). Nevertheless the Malvern produces reproducible results that are suitable for inter-sample comparison and the determination of long-term trends. Moreover, since we generally analyze grain size trends and we do not interpret abundances of the >63 μm fraction and the smaller size fractions, the combination of grain size techniques measuring volume and weight percentages does not impact our interpretations.

Measurements of weight percent $CaCO_3$ were made on samples from Site 690. Analyses were performed at the University of Wisconsin using a CM5240 TIC Autoanalyzer coulometer. Analytical precision of this instrument is ±1% as demonstrated by replicate analyses of a pure carbonate reagent standard. $CaCO_3$ data from Site 1209 and 1262 are from published studies using sim-

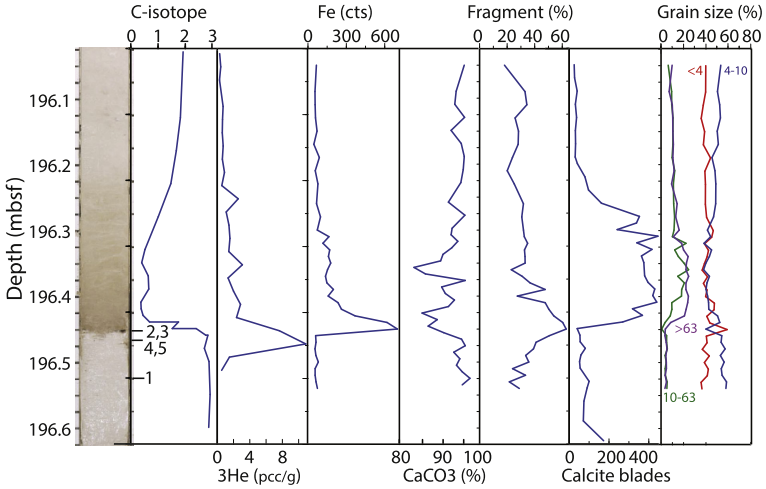

Fig. 3. Lithology, chemical and grain size data from the PETM at Site 1209 (Hole B). Sediments are bioturbated below and above the base of the PETM; a small burrow mixes the pale brown PETM clay-rich ooze into the underlying white chalk indicating minimal bioturbation at the onset of the event. Arrows refer to color changes discussed in text; 1-decline in fragmentation, 2-BFE, 3-CIE, 4-decrease in $CaCO_3$ content, 5-deterioration of nannofossil preservation (see text and Supplemental Materials Table 2). Fe content in counts per second derived by XRF scanning from Westerhold et al. (2008), maximum is 180 cps. Bulk carbonate isotope and fragmentation data from Colosimo et al. (2006). ^{3}He data from this investigation. Calcite blade counts from Gibbs et al. (2006a). Sediments between 196.35 and 196.525 mbsf impacted by syndepositional and burndown dissolution. The ^{3}He data are acquired from the same sample set as other data, but the Fe data were not measured in Hole 1209B but correlated from Site 1209 Holes A and C based on the lithologic boundary. (For interpretation of the references to color in this figure, the reader is referred to the web version of this article.)

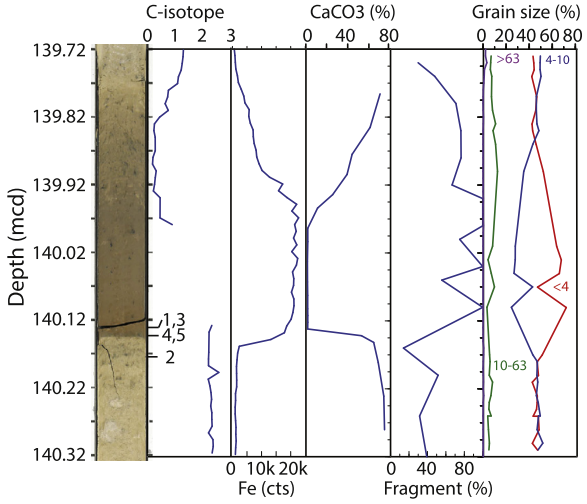

Fig. 4. Lithology, chemical and grain size data from the PETM at Site 1262. The base of the PETM at Site 1262 shows less evidence for bioturbation than the other sites. Arrows refer to color changes discussed in text; 1-decline in fragmentation, 2-BFE, 3-CIE, 4-decrease in $CaCO_3$ content, 5-deterioration of nannofossil preservation (see text and Supplemental Materials Table 2). Fe content in thousand counts per second derived by XRF scanning from Westerhold et al. (2008), maximum is 23,000 cps. Bulk carbonate isotope and carbonate data from Zachos et al. (2005). Fragmentation data from Kelly et al. (2010). Gap in data result from lack of carbonate for isotope measurement. Sediments above 139.98 mcd impacted by syndepositional dissolution; those from 140.13 to 140.21 mcd by burndown dissolution. The boundary between syndepositional and burndown dissolution cannot be delineated. (For interpretation of the references to color in this figure, the reader is referred to the web version of this article.)

ilar instrumentation (Zachos et al., 2005; Colosimo et al., 2006). The total amount of dissolution can be determined from changes in the percent $CaCO_3$ using the technique described in Broecker (1995, 2009). Note that in deep-sea sediments with high carbonate and low terrigenous content, a very large amount of dissolution is required to lower carbonate significantly (Stap et al., 2009). Fragmentation data were derived from Kelly et al. (2005) and unpublished for Site 690, Colosimo et al. (2006) for Site 1209, and Kelly et al. (2010) for Site 1262. X-ray fluorescence Fe data are obtained from Röhl et al. (2000) for Site 690 and Westerhold et al. (2008) for Sites 1209 and 1262. Nannofossil preservation across the PETM at Sites 690 and 1209 was observed in an FEI Quanta 200 Environmental Scanning Electron Microscope in the Mark Wainwright Analytical Centre at the University of New South Wales. The Site 1209 section was studied in a similar fashion by Raffi and De Bernardi (2008) but at lower resolution. Samples in the key interval at Site 1262 lacked $CaCO_3$ and thus were not observed. New He isotope data were obtained on 1 g samples of bulk sediment at Site 1209, using the methods described by Farley and Eltgroth (2003). Extraterrestrial ^{3}He concentrations were determined by deconvolution of the presumed extraterrestrial–terrigenous helium mixture assuming end member ratios of 2.8×10^{-4} and 4×10^{-8} respectively. Because ^{3}He/^{4}He ratios are very high in Site 1209 sediments ($>7 \times 10^{-5}$), the fraction of ^{3}He assigned to an extraterrestrial source ($^3He_{ET}$) always exceeds 99%. The formal uncertainty on $^3He_{ET}$ is better than 5%, though statistical variability in the abundance of individual cosmic dust grains likely contributes additional scatter to the data set (see Farley and Eltgroth, 2003). No samples were replicated.

To directly compare records from the different sites, sample depths are converted to age using published orbital chronologies at Sites 690 and 1262 (Röhl et al., 2007; Westerhold et al., 2008).

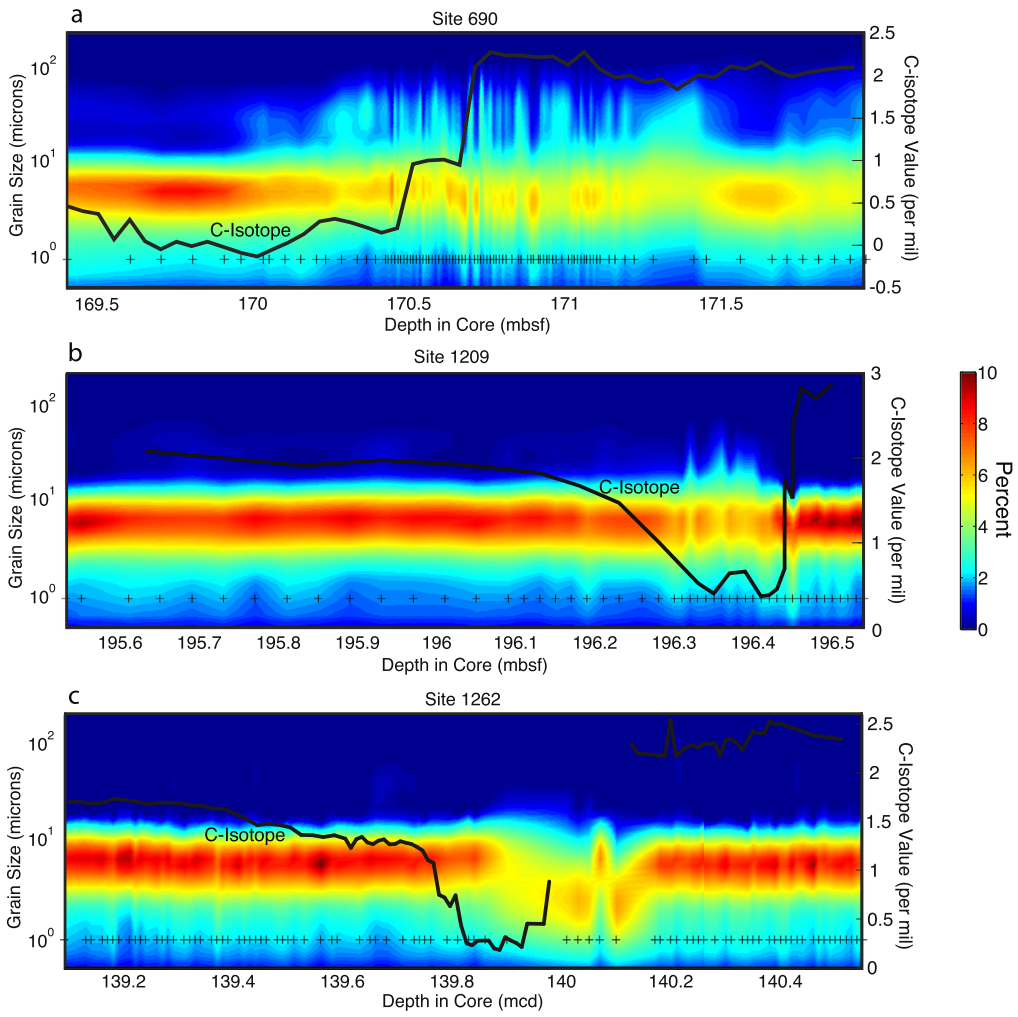

Fig. 5. Grain size data plotted on a logarithmic scale against depth for three PETM records: a. Site 690, b. Site 1209 and c. Site 1262. The figure illustrates the different grain size anomalies at the three sites. Plots are density of percentages interpolated between samples, which are shown with crosses at the bottom of each plot. Also plotted are carbon isotope values (black line; for sources see Fig. 2). Density scale at right. The Malvern Mastersizer has a precision of 0.5–1%.

Orbital cycles are less obvious at Site 1209 (Westerhold et al., 2008) hence we determined the ages of samples by linear interpolation between the bottom and top of the CIE (points A and H from Zachos et al., 2005; 196.45 and 195.93 meters below sea floor (mbsf), respectively). Chronology based on ^{3}He exists for the Site 690 section and is similar to the orbital time scale in the lower part of the PETM (e.g., Farley and Eltgroth, 2003) of interest in the present work. No calibration interval is available for creating an age model using the Site 1209 ^{3}He data, so instead we use $^{3}He_{ET}$ only to assess relative sedimentation rates and the possibility of winnowing.

3. Results

3.1. Grain size data

The grain size data illuminate the composition of sediments in terms of the relative abundance of foraminifera, nannofossils and clay (Figs. 2–6). For the purpose of investigating trends, we divide and denominate the size classes into the following four categories: (i) a "clay fraction" (volume percent <4 μm) dominated by clay minerals that also contains significant amounts of small coccoliths and micarb (pieces of nannofossils and small diagenetic calcite grains), (ii) a "nannofossil fraction" (volume percent 4–10 μm) dominated by coccoliths and other nannoplankton debris, (iii) a 10–63 μm fraction (volume percent) composed of a mixture of large nannofossils, coccospheres, and small or fragmented foraminiferal tests, and (iv) a "foraminiferal fraction" consisting of sand-sized grains (weight percent >63 μm measured by wet sieving) that is generally dominated by foraminiferal tests. Even though the cutoffs for these different size classes are somewhat subjective, their definition helps us describe meaningful trends in the sediment-size distributions of samples. Because the <63 μm grain size groupings are calculated from a total of 100%, significant increases in the proportion of one size fraction will be offset by decreases in the proportions of the other size fractions (Figs. 2–5), the well-established closed-sum effect.

Apart from the PETM interval, the data show that sediments at Sites 1209 and 1262 are dominated (50–60%) by the nannofossil size fraction (volume % 4 to 10 μm), with a subsidiary amount from the <4-μm fraction (Figs. 3, 4). Site 690 sediments generally contain a greater proportion of the <4 μm and 10–63 μm fractions, and a slightly lower nannofossil size fraction (~30–40%; Fig. 2) than at the other sites.

Against this backdrop, the PETM interval, as defined by the CIE, shows a unique anomaly in grain-size distribution at each site (Figs. 2–6). The anomaly at Site 1262 involves an increase in the relative abundance of the clay (volume % <4 μm) size fraction, a decrease in the nannofossil fraction (volume % 4–10 μm), and no concomitant increase in the foraminiferal (weight % >63 μm) fraction (Figs. 4, 5c). At Site 1209, the anomaly also includes a de-

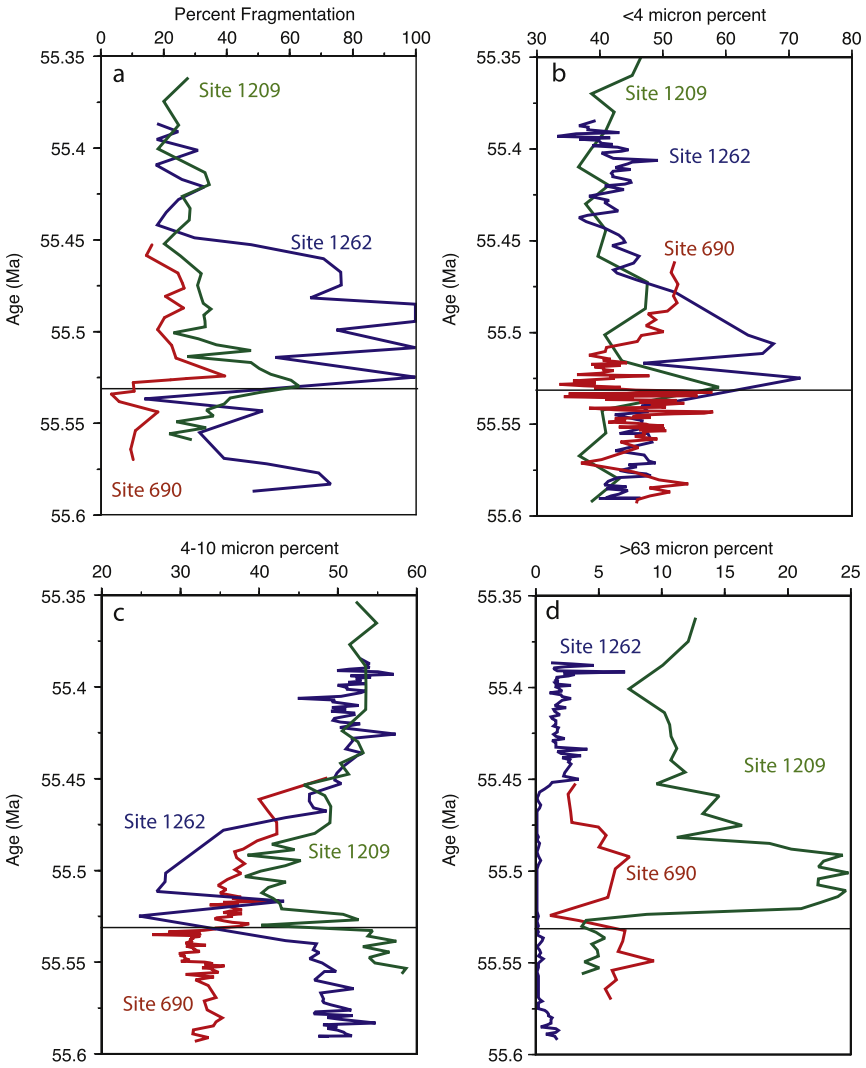

Fig. 6. a. Foraminiferal fragmentation percentage, b. clay (volume % <4 μm), c. nannofossil (volume % 4–10 μm), and d. coarse fraction (weight % >63 μm) versus age for the three study sites. Samples are converted to age using orbital stratigraphy (Site 690, Röhl et al., 2007; Site 1262, Westerhold et al., 2008) and assuming constant sedimentation rates (Site 1209). Black line delimits the base of the CIE.

crease in the proportion of the dominant nannofossil (volume % 4 – 10 μm) size fraction and an increase in the relative abundances of clay (volume % <4 μm), but an increase in the foraminiferal (weight % >63 μm) size fraction (Figs. 3, 5b). The anomaly at Site 690 is more subtle, involving a slight increase in the mean grain size and a broadening of the dominant nannofossil fraction size distribution from 4–10 μm to 4–15 μm (Figs. 2, 5a). This may reflect influx of thick-shelled, robust Acarininid foraminifera (Kelly, 2002).

The weight percent >63-μm fraction at the three sites is characterized by different values and trends (Kelly et al., 2005; Colosimo et al., 2006; Kelly et al., 2010; Fig. 6d). At Site 690 values initially drop then remain relatively constant between 5 and 9%. The trend at Site 1209 shows low values of 4–9% at the base, a sharp increase to 21–25% just above the base of the CIE, followed by values generally between 10–15%. Finally, at Site 1262, values are generally between 1–4% except within the CIE where they are close to 0%.

3.2. Dissolution proxy data

Fragmentation values increase at different stages of the PETM in the study sites (Kelly et al., 2005, 2010; Colosimo et al., 2006; Fig. 6a). At Site 690, the key feature is a gradual increase in fragmentation just above the CIE onset from a minimum of 3% to 39% (Figs. 2, 6a). At Site 1209 values increase abruptly from 41% to 63% beginning 8 cm below the CIE (Figs. 3, 6a). At Site 1262 the key feature is an abrupt increase from 14% to 100% beginning a few cm below the CIE (Figs. 4, 6a); samples without foraminifera at Site 1262 technically have a fragmentation value of infinity (Leon-Rodriguez and Dickens, 2010) but for graphical purposes are assigned a value of 100%. Fragmentation levels are considerably higher, and the PETM increase is much more abrupt, at Sites 1209 and 1262 than at Site 690 (Fig. 6a).

Published data for all three sites show the distinctive excursion in bulk carbon isotope values and decreases in $CaCO_3$ contents (Figs. 2–4), although the shapes of the curves for both variables differ substantially between sections. The new high-resolution $CaCO_3$ data from Site 690 show values between 76 and 90% below 170.79 mbsf, followed by a gradual decrease to ~61% at 170.58 mbsf, succeeded by gradually increasing values up to 87% at 169.5 mbsf (Fig. 2). Estimates of percent dissolution ranges from ~60% at Site 690 to 100% at Site 1262 (Fig. 7). Published high-resolution Fe records show sharp increases corresponding to the base of the clayey nannofossil ooze at Site 1209 and claystone at Site 1262, but a more gradual increase at Site 690 (Figs. 2–4).

Nannofossil preservation at Site 690 is generally poor to moderate with a significant amount of dissolution of rims and cen-

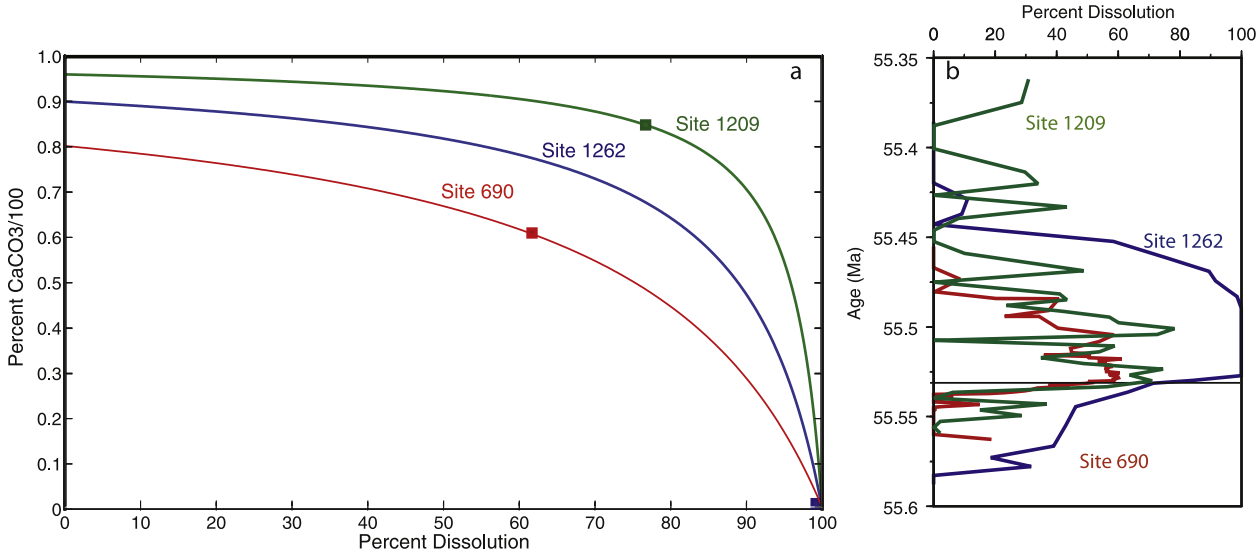

Fig. 7. a. Estimates of percentage dissolution for the three PETM records based upon the technique described in Broecker (1995). Initial $CaCO_3$ percentages are representative values just below the PETM: 96% (Site 1209), 90% (Site 1262), and 80% (Site 690). Squares represent estimates of maximum dissolution based on lowest $CaCO_3$ percent. b. Estimates of dissolution % plotted versus depth at the three sites.

tral areas of specimens (Supplemental Materials, Plate 1). Samples from below the PETM interval, near the base of the study section, show high nannofossil relative abundance and moderate degree of dissolution. There is a gradual deterioration in nannofossil preservation between 170.80 mbsf (moderate dissolution with samples dominated by coccoliths and larger pieces of coccoliths) and 170.75 mbsf (severe dissolution with lower numbers of coccoliths and increased micarb and clay content) (Supplemental Materials, Plate 1). This is followed by generally poor preservation with a lower number of coccoliths up to 170.70 mbsf. There is another substantial deterioration in preservation, involving a decrease in the relative abundance of coccoliths and an increase in the amount of micarb and clay, between 170.70 mbsf and 170.68 mbsf (Supplemental Materials, Plate 1). This is followed by an interval dominated by micarb and clay with few whole coccoliths and generally very poor preservation up to 170.65 mbsf. There is a slight improvement in preservation in the sample at 170.64 mbsf, and samples above that level generally have more coccoliths than samples below.

Nannofossil preservation in samples from immediately below the PETM and in the early part of the event at Site 1209 is generally better than at Site 690 with less pervasive dissolution but slightly more overgrowth, and generally lower amounts of micrite and clay (Supplemental Materials, Plate 2). In general, there is a moderate decline in nannofossil preservation and a decrease in relative abundance between 196.47 to 196.46 mbsf (just below the CIE), and preservation remains poor to moderate for the remainder of the interval studied.

The PETM interval at all three sites shows evidence of bioturbation, with intensity differing between locations. Sediments from throughout the lower PETM at Site 690 are moderately bioturbated with white and pale gray burrows (Fig. 2). Site 1209 also is bioturbated below and above the base of the PETM; preservation of the contact between the pale brown PETM clay rich ooze and underlying white chalk with a small burrow suggests minimal bioturbation at the onset of the event (Fig. 3). The PETM interval at Site 1262 shows less evidence for bioturbation than the other sites, especially in the lower part of the claystone and across the contact with the underlying chalk (Fig. 4).

4. Discussion

4.1. Impacts of dissolution on grain size distributions

The calcareous microfossil components of deep-sea sediments such as those deposited during the PETM are extraordinarily variable in size and shape. Foraminifera are large (generally >63 μm), hollow, and largely porous. Nannoplankton are generally preserved as much smaller (~4–10 μm) and solid plates. The impact of dissolution on these particles is complex and poorly understood.

The PETM is associated with unique grain size anomalies at the three study sites (Fig. 5); here we address how these changes relate to dissolution during the event. The abrupt increase in foraminiferal fragmentation at the sites is clear evidence for intensified dissolution during the PETM (e.g., Hancock and Dickens, 2006; Colosimo et al., 2006; Kelly et al., 2010). Relative fragmentation values and estimates of percent dissolution (Figs. 6a, 7) delineate a gradient in dissolution intensity from least severe at Site 690 to intermediate at Site 1209 and most severe at Site 1262; this gradient serves as a basis for interpreting the PETM grain size anomalies.

At Sites 1209 and 1262 when dissolution increases, as indicated by higher fragmentation levels, clay fraction increases and $CaCO_3$ content decreases as expected (Figs. 3, 4, 6b). At Site 1209, extraterrestrial ^{3}He concentration also increases at this time (no ^{3}He data are available for Site 1262) again consistent with dissolution and carbonate removal. Significant decreases in the nannofossil (volume % 4–10 μm) and foraminiferal (weight % >63 μm) size fractions occur in the interval of high fragmentation at Site 1262 indicating that dissolution was responsible for the size changes and absence of microfossils during the peak of the PETM (Fig. 4). At Site 1209, the nannofossil fraction decrease is in step with the increase in fragmentation (Fig. 3) suggesting control by dissolution. However, the foraminiferal fraction increases in this interval, reflecting the rise in the relative abundance of large, robust specimens of the genus *Morozovella* (e.g., Kaiho et al., 2006; Petrizzo, 2007). One possibility is that foraminifera were enriched by winnowing, an explanation that is explored in Section 4.3.

At Site 690, the relationships between fragmentation, $CaCO_3$ and clay content are complex (Fig. 2), suggesting that other factors besides dissolution, such as run-off from Antarctica and changes

in plankton productivity were involved (e.g., Robert and Kennett, 1994; Kelly et al., 2005). Moreover, increasing fragmentation levels in the early part of the PETM correspond to an increase in the nannofossil fraction (Fig. 2) involving a pulse of larger, solution-resistant tropical genera such as *Discoaster* (Bralower, 2002; Dedert et al., 2014). This pulse is a partial response to PETM warming but may also reflect poorer nannofossil preservation.

Increases in the abundance of nannofossils at Site 690 and foraminifera at Site 1209 during the PETM are inconsistent with intensified dissolution. In addition, electron microscope observations of nannofossil preservation at Sites 690 and 1209 are difficult to reconcile with fragmentation data. Nannofossil preservation at Site 690 is generally poorer than at Site 1209 (Supplemental Materials Plates 1, 2), even though foraminiferal fragmentation is lower. In summary, the grain size anomaly at Site 1262 is a clear indication of complete $CaCO_3$ dissolution. The anomalies at the other sites are a response to changing faunal and floral composition, which causes different dissolution responses from nannofossils and foraminifera, as well as a more complex dissolution process during deposition and burial. We explore reasons for this complexity in the following section.

4.2. The significance and mechanics of chemical erosion during the PETM

Environmental changes during the PETM occurred rapidly, at least on geological timescales, thus assemblage and stable isotope investigations have been conducted often at cm-resolution (e.g., Kelly, 2002; Thomas et al., 2002; Zachos et al., 2003). With such high-resolution data, consideration must be given to the potential for chemical erosion to erase key stratigraphic intervals and alias biotic and proxy records, including C-isotopes and $CaCO_3$. Alteration of the latter proxy records is especially significant as it may obscure interpretation of the magnitude of the carbon input and the dissolution pulse during the PETM (e.g., Dickens et al., 1997; Zeebe and Zachos, 2007, 2013; Zeebe et al., 2009; Panchuk, 2007; Cui et al., 2011; Fig. 7). Here we constrain the impact of chemical erosion on PETM stratigraphy by integrating grain size and proxy data, electron microscopy, ^{3}He concentrations, and lithostratigraphy.

Before we interpret the data, we briefly consider the mechanics of chemical erosion. A major decrease in deep ocean saturation, as occurred at the onset of the PETM, had two possible impacts; first, it dissolved biogenic $CaCO_3$ settling to the sea floor and within the benthic transition layer—the interval that was actively bioturbated (here termed syn-depositional dissolution), and, second, once all of the carbonate was removed from the benthic transition layer, it dissolved $CaCO_3$ from underlying layers (burndown dissolution). Syn-depositional and burndown dissolution are part of a continuum. If the supply of new $CaCO_3$ to the benthic transition layer is sufficient, then syn-depositional dissolution is continuous and dissolution of existing carbonate via burndown is inhibited. Where $CaCO_3$ supply is lower and burndown is active, however, the process might eventually be limited by development of a thick clay layer that acts as a barrier to fluid migration (e.g., Zeebe and Zachos, 2007). Model studies demonstrate the effect of bioturbation on chemical erosion during the PETM. Active bioturbation supplies new $CaCO_3$ to the sediment surface for syn-depositional dissolution, thus limiting burndown; however, where bioturbation is reduced or non-existent, then dissolution of existing carbonate via burndown occurs (e.g., Zeebe and Zachos, 2007; Panchuk et al., 2008; Kirtland Turner and Ridgwell, 2013). We postulate that winnowing of sediment by bottom currents also limits burndown by supplying carbonate for syn-depositional dissolution.

How can sediments altered by syn-depositional dissolution and burndown be distinguished? Syn-depositional dissolution sediments are characterized by excursion C-isotope values since they are comprised of carbonate deposited during the PETM. The upper part of the syn-depositional dissolution interval is usually calcareous but the base may become non-calcareous as carbonate is depleted just before the onset of burndown. Sediments that have experienced burndown dissolution should be largely non-calcareous, and, where measurable, contain pre-excursion C-isotope values since they predate the PETM. They may also be expected to have higher extraterrestrial ^{3}He concentrations compared to directly underlying (not chemically eroded) sediments owing to the removal of carbonate.

Approximately 15 cm (139.96–140.11 mcd) across the base of the PETM at Site 1262 is devoid of $CaCO_3$ preventing precise definition of the base of the CIE; however, this horizon lies above the uppermost level with pre-excursion C-isotope values (140.13 mcd; Figs. 4, 5c; Supplemental Materials Table 2). The upper part of the non-calcareous interval above 139.98 mcd contains excursion isotope values suggesting syn-depositional dissolution during the PETM. The gap in the C-isotope record does not allow delineation of the boundary between syn-depositional dissolution and burndown sediments, but it is likely that much of the non-calcareous interval was produced by burndown dissolution. The base of the burndown interval can be defined in several ways: (1) the nannofossil fraction shows a gradual decrease in volume combined with fining upward size distribution between 140.10 to 140.18 mcd (Fig. 5c); (2) fragmentation data demonstrate a sharp increase between 140.10 and 140.16 mcd (Fig. 4); and (3) carbonate shows a modest decrease between 140.16 and 140.21 mcd, and a sharp drop at 140.14 mcd (Fig. 4). These data suggest at least 8 cm (140.13–140.21 mcd) and likely closer to 23 cm (139.98–140.21) of burndown. The interval beneath the claystone contains evidence for partial but not complete dissolution (Fig. 4), suggesting that the claystone was not a barrier to dissolution and that burndown does not remove all carbonate. In fact, Kelly et al. (2010) proposed that burndown progressed 40 cm below the CIE at Site 1262 based on decreases in coarse fraction and increases in solution-resistant benthic foraminifera, thus our estimate may be a minimum. The preservation of the lithologic boundary at the onset of the PETM at Site 1262 (Fig. 4) suggests that bioturbation was suppressed which would have exacerbated the impact of burndown (Panchuk et al., 2008; Fig. 8).

The lithologic boundary and abrupt chemical shifts across the base of the PETM at Site 1209 are similar to Site 1262, but $CaCO_3$ contents remain above 85% (Fig. 3). High fragmentation levels and lower carbonate levels up to 196.36 mbsf within the CIE interval are evidence for syn-depositional dissolution. Below the base of the CIE, these same signals are evidence for burndown. Colosimo et al. (2006) identified a 7.5 cm-interval of burndown between the base of the CIE, the PETM claystone and the BFE (Takeda and Kaiho, 2007), all at 196.45 mbsf, and the increase in fragmentation values at 196.525 mbsf. Grain size data also show a minor decrease in the nannofossil fraction over the same interval (down to 196.53 mbsf; Fig. 3). Dissolution of a substantial amount of $CaCO_3$ is supported by the abundance of diagenetic blades of calcite, which likely precipitated once saturation levels recovered (Fig. 3; Supplemental Materials Plate 3a, b; see also Kozdon et al., 2013). Similarly, the extraterrestrial ^{3}He concentration rises beginning at $\sim$196.5 mbsf, again consistent with burndown and carbonate removal. Yet, the preservation of nannofossils deteriorates only slightly within the PETM (Supplemental Materials Plate 2). Thus sediments from Site 1209 combine evidence for limited as well as intensive dissolution. How can these conflicting signals be explained? The magnitude of the ^{3}He peak at Site 1209 is indicative of a significant amount of time straddling the syn-depositional and burndown intervals across the base of the CIE (Fig. 3). Bioturbation was active in this interval (Fig. 3), and, as discussed, enrichment of the

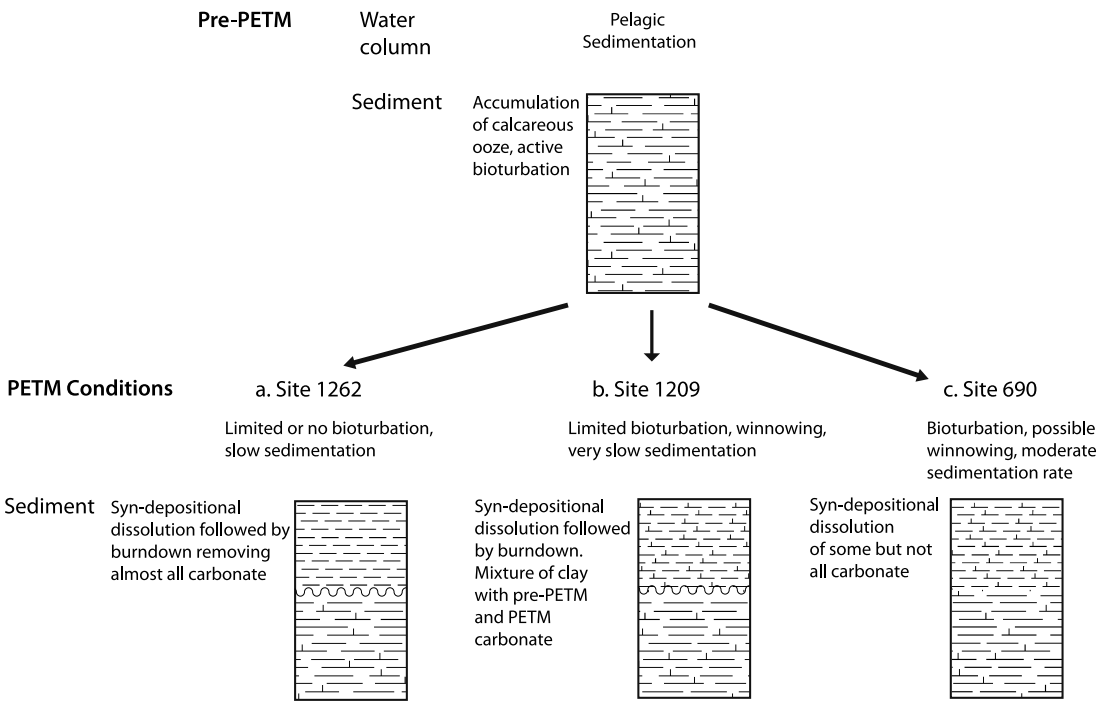

Fig. 8. Cartoons illustrating hypothesis for the variable impact of chemical erosion on stratigraphy at Sites 690, 1209 and 1262.

foraminiferal size fraction in the lower part of the PETM could be a result of winnowing. Thus we postulate that foraminifera and nannoplankton that accumulated prior to and after burndown and syn-depositional dissolution were mixed by bioturbation and winnowing together with clay that accumulated during the extended interval of dissolution and calcite blades that precipitated after dissolution ceased and saturation increased.

The removal of $CaCO_3$ via dissolution near the base of the PETM at Site 1209 and 1262 produced a highly condensed stratigraphy as supported by the near coincidence of changes in preservation, $CaCO_3$, and the BFE with the base of the CIE (Figs. 3, 4; Zachos et al., 2005; Takeda and Kaiho, 2007; Raffi and De Bernardi, 2008). At Site 690, by comparison, the decline in nannofossil preservation (170.75–170.80 mbsf), increase in fragmentation (170.60 mbsf), shift in $CaCO_3$ content (170.79 mbsf), changes in the relative proportion of different grain sizes, the BFE (170.60–170.61 mbsf; Thomas, 2003), and the bulk CIE (170.70 mbsf) (we use the definition of Thomas et al., 2002; see Supplemental Materials), are distributed over 20 cm of section (Fig. 2; Supplemental Materials Table 2). Most significantly, the decrease in $CaCO_3$ begins 9 cm below the base of the CIE.

The PETM onset at Site 690 does not exhibit sharp lithologic boundaries as seen in the other sites. Two subtle color changes at 170.77 and 170.63 mbsf coincide with shifts in Fe and $CaCO_3$, suggesting minor changes in sediment composition (Fig. 2). There is no clear evidence for substantial burndown: the section is completely calcareous and ^{3}He increases only by a factor of ~2–3 above pre-event levels, compared to the ~10× change seen at Site 1209 (Farley and Eltgroth, 2003; Figs. 2, 3). Changes in carbonate content and nannofossil preservation are subtle. The onset of dissolution at Site 690 appears to have been sequential with the first step at 170.79 mbsf as indicated by the decrease in $CaCO_3$ content and the decline in nannofossil preservation between 170.80–170.75 mbsf (Supplemental Plate 1) and the second step at 170.60 mbsf as indicated by the increase in foraminiferal fragmentation (Fig. 2). A similar stepped pattern can be inferred from the Site 690 ^{3}He concentrations at Site 690 (Farley and Eltgroth, 2003).

The dissolution history at Site 690 is likely connected to the propagation of carbon from the surface to deep ocean. The pulse of C is thought to have entered the surface ocean as indicated by the C-isotope shift in planktonic foraminifera at 170.785 mbsf, close to the first step in dissolution, and reached the deep sea, signaled by the first excursion C in benthic foraminifera at 170.675 mbsf (Thomas et al., 2002) prior to the second step. We postulate that the first dissolution step signified the onset of syn-depositional dissolution in the water column, and the second dissolution step the onset of dissolution in the benthic transition zone. However, the amount of micrite in all samples (Supplemental Materials Plate 1) suggests that dissolution and reprecipitation continued well after deposition. Nannofossils are generally more dissolved at Site 690 than at Site 1209; we therefore postulate that the peak dissolution horizon at Site 690 has been preserved whereas at Site 1209 it has been removed by more intensive chemical erosion. We speculate that the 14 cm interval between 170.63 and 170.77 mbsf corresponds to the highly condensed section at the base of the PETM at Sites 1209 and 1262 (Figs. 2–4).

How can the preservation of the expanded PETM section at Site 690 be explained? We postulate that downwelling delivered young, relatively saturated, deep waters during the event (Thomas et al., 2003), explaining the gradual decrease in saturation at this site. Sedimentation rate in the pre-PETM interval at Site 690 was considerably higher than at the other sites, 2.3 cm/kyr versus 0.8 cm/kyr at Site 1262 and 0.3 cm/kyr at Site 1209 (Röhl et al., 2007; Westerhold et al., 2007, 2008). Thus, sufficient pelagic flux combined with bioturbation, and possibly winnowing, supplied carbonate to the seafloor at a faster rate than it was dissolved, tempering chemical erosion during the early part of the PETM (Fig. 8).

Because the study sections appear to represent a range of chemical erosion intensity, our results can be extended to other PETM sections. Sites that contain clay or claystone with close to 0% $CaCO_3$ and an abrupt lithologic boundary, as at Site 1262 and the other Walvis Ridge PETM sections, are likely characterized by intense burndown. At other sites where the lithologic boundary is abrupt, but $CaCO_3$ decreases to levels well above 0%, as at

Site 1209 and the other Shatsky Rise PETM sections, bioturbation and/or slow sedimentation, combined with syn-depositional dissolution and burndown, have mixed or erased the interval of most severe dissolution. Thus $CaCO_3$ data from these sites (Fig. 7) underestimate the amount of dissolution. Finally, at sites where the lithologic boundary is more gradual and the $CaCO_3$ decrease is moderate, as at Site 690 and nearby Site 689 (Zachos et al., 2007), bioturbation and more moderate $CaCO_3$ accumulation rates may have diminished the severity of chemical erosion, likely precluding burndown, and, potentially preserving the onset of the PETM.

4.3. The impact of bioturbation, winnowing and dissolution on the fidelity of Site 690 assemblage and isotopic records

We have described how bioturbation and winnowing have impacted dissolution during the PETM. In this section, we consider how all three processes have affected proxy records. Both bioturbation and winnowing have the potential to bias microfossil-based proxy records, especially those collected at cm-level resolution. Winnowing suspends clay and clay-sized carbonate, and typically leads to an increase in the volume of silt and sand, and a steepening of the coarse limb of the grain-size distribution (Kranck et al., 1996). Where currents are particularly strong, and the sand fraction is increased significantly, a bimodal grain size distribution may develop (McCave et al., 1995). Thus grain size data can be used to identify evidence for winnowing.

Site 690 samples contain a significant foraminiferal fraction (Figs. 2, 5a, 6d) and the possibility exists that foraminifera have been preferentially enriched by winnowing. However, unless current speeds are extremely constant over time, which is unlikely, winnowing would not produce homogeneous grain size distributions, and, with a few exceptions, the distributions of Site 690 samples are relatively similar (Supplemental Materials Fig. 3). A few samples have somewhat more bimodal distributions with enrichment of the coarse silt fraction. Removal of fine fraction during winnowing could have produced the silt fraction peak in these samples, but no steepening of the coarse limb of the grain-size distribution is observed.

At Site 690, a temporal series of events in single-specimen planktic and benthic foraminiferal carbon and oxygen isotope values is observed between 170.81 and 170.70 mbsf; this series of events has been interpreted in terms of the progression of PETM warming and mixing of carbon from the surface ocean down towards the seafloor (Thomas et al., 2002). Nearly the same interval is characterized by consecutive shifts in planktic foraminifera, nannofossils and benthic foraminifera that also have been interpreted as progressive changes in planktic and benthic habitats (Bralower, 2002; Kelly, 2002; Thomas, 2003). The carbon isotope shift in the (nannofossil-dominated) bulk carbonate fraction corresponds in timing and magnitude ($\sim$2‰) with the CIE measured on the thermocline-dwelling foraminifera, *Subbotina*; however, given their shallow habitat, nannoplankton should carry the same isotope signal as the surface-dwelling planktic foraminifera genus, *Acarinina* which records a CIE of $\sim$4‰. The offset between *Acarinina* single specimen and bulk isotope data at Site 690, and the magnitude of the marine CIE in general, have received significant discussion but remain enigmatic (see Stoll, 2005; McCarren et al., 2008; McInerney and Wing, 2011).

One explanation for the CIE offset at Site 690 is that peak PETM C-isotopic values of *Acarinina* were reduced by the loss of photosymbionts as a result of abrupt warming, as has been proposed for the Middle Eocene Climatic Optimum (Edgar et al., 2013). Other explanations are that the surface water shifts reflect normal interannual to millennial variation (Kent et al., 2003), that relatively smaller nannofossils were winnowed up-section with respect to the relatively larger foraminifera or preferentially dissolved and overgrown (Zachos et al., 2007), that the dominant nannoplankton live deeper in the water column (Schueth and Bralower, submitted for publication), or that foraminifera were preferentially burrowed down section by size differential bioturbation (e.g., Thompson et al., 1995; Thomas, 2003; Stoll, 2005; Sluijs et al., 2007b).

The impact of bioturbation and winnowing on the Site 690 single specimen isotope record can also be assessed from the distribution of foraminiferal shells bearing pre-excursion and excursion C-isotope values (e.g., Stott, 1992; Kelly et al., 1996; Thomas et al., 2002). Individual "outlier" shells with pre-PETM isotope values are present in samples in which the majority of specimens shows excursion isotope values and vice versa (see details in Supplemental Materials and Supplemental Materials Fig. 2). In this way single specimen values suggest the combination of bioturbation and winnowing has the potential to mix foraminiferal specimens by up to 20 cm upward or downward from their original positions. However, the rarity of these clear outliers (only 10 of 483 total shells analyzed by Thomas et al., 2002, have isotope values significantly offset from others in the same samples) and the preservation of the multiple abrupt carbon and oxygen isotope shifts in surface and thermocline foraminifera (Supplemental Materials Fig. 2) indicates that most shells have not been mixed upwards or downwards by winnowing and/or bioturbation by more than a centimeter or two, and the specimens that have been moved further are likely contaminated during drilling. Site 1209 shows evidence for more limited bioturbation than Site 690, especially across the base of the claystone unit (Fig. 3). Accordingly, the distribution of single specimen isotope values shows no obvious evidence for mixing (Zachos et al., 2003). Grain size distributions show anomalously coarse samples between 196.40 and 196.32 mbsf (Supplemental Materials Fig. 3). Although these samples do not possess distributions such as a coarse limb or bimodality, the abrupt top and base of the 8-cm coarse interval is possible evidence for winnowing.

The impact of bioturbation on the fine fraction at Site 690 can also be constrained from bulk stable isotope records. The archive half of the Site 690 PETM likely sampled a burrow, explaining the 7-cm lower and gradual onset of the bulk CIE (Thomas et al., 2002) compared to the sharp decrease in the working-half (Bains et al., 1999) (Supplemental Materials Fig. 4). The 7-cm offset provides an estimate of potential vertical mixing of the nannofossil-dominated bulk sediment fraction by bioturbation. Bioturbation could explain the separation of isotopic signals carried by nannoplankton (i.e. bulk) and those carried by foraminifera, however nannofossils would be mixed further downward than foraminifera, which is the opposite to observations at Site 690 (e.g., Stoll, 2005). Winnowing, on the other hand, could have mixed nannofossil signals upwards with respect to foraminiferal signals, but it would result in gradual shifts rather than the abrupt ones observed in the nannofossil assemblage records (e.g., Bains et al., 1999; Bralower, 2002). The general lack of evidence for impact of bioturbation and winnowing on the biotic and stable isotopic records in the PETM at Site 690 is supported by discovery of the same progression of surface to bottom single specimen isotope signals at nearby Site 689 (Zachos et al., 2007).

Syn-depositional dissolution at Site 690 during the early part of the PETM may, in fact, offer a potential explanation for the offset in timing and magnitude between bulk and *Acarinina* single specimen isotopes, as postulated by Zachos et al. (2007). Although single foraminiferal specimens have likely been overprinted by diagenesis, the majority of their calcite and stable isotope values are original. The co-existing bulk carbonate includes substantial micrite (Supplemental Materials Plate 1) potentially reprecipitated from $CaCO_3$ dissolved at and below the seafloor, with the former component containing pre-excursion isotope values obtained from diffusion from below. The mixture of nannofossils and repre-

cipitated carbonate is a potential explanation of the significantly smaller bulk carbon isotope shift magnitude (~2‰) compared to the ~4‰ shift measured in *Acarinina* (Thomas et al., 2002). However, this explanation does not resolve the difference in CIE magnitude between *Acarinina* and *Subbotina*, thus loss of *Acarinina* photosymbionts remains as a viable alternative.

At Site 690, the bulk CIE lies ~9 cm above the initial carbonate decline and assemblage change (Kelly, 2002). At the other two sites, the main isotopic and microfossil shifts (Zachos et al., 2003; Gibbs et al., 2006b; Petrizzo, 2007), the $CaCO_3$ decrease and fragmentation increase, lie within 1–2 cm (Fig. 2), again suggesting that key parts of these PETM records have been chemically eroded. By comparison, Site 690, and neighboring Site 689, may be unusual in the preservation of the vital, earliest intervals of the PETM.

5. Conclusions

The PETM shows an abrupt but unique grain size anomaly at each of three sites characterized by a range of dissolution intensity during the event. These anomalies provide a measure of the sediment fractions lost as a result of dissolution. Combined with lithology, microscopic observation, $CaCO_3$, ^3He, and fragmentation data, the grain size anomalies suggest that chemical erosion has had a variable impact on the record of the event at each site. The results indicate that sites typified by slower carbonate accumulation and less intense bioturbation are characterized by dissolution of pre-existing sediments or burndown, as also suggested by models. The sites characterized by faster carbonate accumulation and more active bioturbation, and possibly winnowing, are characterized by syn-depositional dissolution but apparently not by burndown, and, as a result, have preserved a more complete PETM sequence. Grain size data indicate that winnowing has not had a significant effect on proxy records in PETM sections. The composition of nannofossil and planktonic foraminiferal assemblages, and in particular, the solution susceptibility of the dominant species, also control dissolution during the PETM.

Acknowledgements

We thank Jenny Norman of the Mark Wainwright Analytical Centre, University of New South Wales for assistance with electron microscopy. We thank Lee Kump, Andy Ridgwell and Sandra Kirtland Turner for insightful discussions, Thomas Westerhold for stratigraphic information, and Jerry Dickens and two anonymous reviews for very constructive and extremely helpful critique and advice. This research used samples provided by the Integrated Ocean Drilling Program (IODP). Research funded by the National Science Foundation (EAR06-28394) to Bralower and (OCE-1060877C) to Farley.

Appendix A. Supplementary material

Supplementary material related to this article can be found online at http://dx.doi.org/10.1016/j.epsl.2014.05.055.

References

Agnini, C., Fornaciari, E., Rio, D., Tateo, F., Backman, J., Giusberti, L., 2007. Responses of calcareous nannofossil assemblages, mineralogy and geochemistry to the environmental perturbations across the Paleocene/Eocene boundary in the Venetian Pre-Alps. Mar. Micropaleontol. 63, 19–38. http://dx.doi.org/10.1016/j.marmicro.2006.10.002.

Archer, D., Kheshgi, H., Maier-Reimer, E., 1997. Multiple timescales for neutralization of fossil fuel CO_2. Geophys. Res. Lett. 24, 405–408.

Archer, D., Kheshgi, H., Maier-Reimer, E., 1998. Dynamics of fossil fuel CO_2 neutralization by marine $CaCO_3$. Glob. Biogeochem. Cycles 12, 259–276.

Arrhenius, G., 1952. Sediment cores from the East Pacific. In: Pettersson, H. (Ed.), Rep. Swed. Deep-Sea Exped., 1947–1948, vol. 5, pp. 189–201.

Bains, S., Corfield, R.M., Norris, R.D., 1999. Mechanisms of climate warming at the end of the Paleocene. Science 285, 724–727.

Beaufort, L., Probert, I., de Garidel-Thoron, T., Bendif, E.M., Ruiz-Pino, D., Metzl, N., Goyet, C., Buchet, N., Coupel, P., Grelaud, M., Rost, B., Rickaby, R.E.M., de Vargas, C., 2011. Sensitivity of coccolithophores to carbonate chemistry and ocean acidification. Nature 476, 80–83. http://dx.doi.org/10.1038/nature10295.

Berger, W., Winterer, E.L., 1974. Plate stratigraphy and the fluctuating carbonate line. In: Pelagic Sediments: On Land and Under the Sea, pp. 11–48.

Bralower, T.J., 2002. Evidence for surface water oligotrophy during the late Paleocene thermal maximum: nannofossil assemblage data from Ocean Drilling Program Site 690, Maud Rise, Weddell Sea. Paleoceanography 17. http://dx.doi.org/10.1029/2001PA000662.

Bralower, T.J., Premoli Silva, I., Malone, M.J., 2006. Leg 198 synthesis: a remarkable 120-m.y. record of climate and oceanography from Shatsky Rise, northwest Pacific Ocean. In: Bralower, T.J., Premoli Silva, I., Malone, M.J. (Eds.), Proc. ODP, Sci. Results. College Station, TX. In: Ocean Drilling Program, vol. 198, pp. 1–47.

Bralower, T.J., Eccles, L., Kutz, J., Yancey, T., Schueth, J., Arthur, M., Bice, D., 2010. Grain size of Cretaceous–Paleogene boundary sediments from Chicxulub to the Open Ocean: implications for interpretation of the Mass Extinction Event. Geology 38, 199–202.

Broecker, W., 1995. The Glacial World According to Wally. Eldigio Press.

Broecker, W., 2009. Wally's quest to understand the ocean's $CaCO_3$ cycle. Annu. Rev. Mar. Sci. 1, 1–18. http://dx.doi.org/10.1146/annurev.marine.010908.163936.

Broecker, W.S., Clark, E., 1999. $CaCO_3$ size distribution: a paleo carbonate ion proxy. Paleoceanography 14, 596–604.

Broecker, W.S., Takahashi, T., 1977. Neutralization of fossil fuel CO_2 by marine calcium carbonate. In: Anderson, N.R., Malahoff, A. (Eds.), The Fate of Fossil Fuel CO_2 in the Oceans. Plenum, New York, pp. 213–241.

Caldeira, K., Wickett, M.E., 2005. Ocean model predictions of chemistry changes from carbon dioxide emissions to the atmosphere and ocean. J. Geophys. Res. 110 (C9), C09S04.

Chiu, T.-C., Broecker, W.S., 2008. Toward better paleocarbonate ion reconstructions: new insights regarding the $CaCO_3$ size index. Paleoceanography 23, PA2216. http://dx.doi.org/10.1029/2008PA001599.

Colosimo, A., Bralower, T.J., Zachos, J., 2006. Evidence for lysocline shoaling at the Paleocene/Eocene thermal maximum on Shatsky Rise, Northwest Pacific. In: Bralower, T.J., Premoli-Silva, I., Malone, M.J., et al. (Eds.), Proc. ODP Sci. Res., vol. 198, pp. 1–36.

Crouch, E.M., Heilmann-Clausen, C., Brinkhuis, H., Morgans, H.E.G., Rogers, K.M., Egger, H., Schmitz, B., 2001. Global dinoflagellate event associated with the late Paleocene thermal maximum. Geology 29, 315–318.

Cui, Y., Kump, L.R., Ridgwell, A.J., Charles, A.J., Junium, C.K., Diefendorf, A.F., Freeman, K.H., Urban, N.M., Harding, I.C., 2011. Slow release of fossil carbon during the Palaeocene–Eocene thermal maximum. Nat. Geosci. 4, 481–485. http://dx.doi.org/10.1038/NGEO1179.

Dedert, M., Stoll, H., Kars, S., Young, J.R., Shimizu, N., Kroon, D., Lourens, L., Ziveri, P., 2014. Temporally variable diagenetic overgrowth on deep-sea nannofossil carbonates across Palaeogene hyperthermals and implications for isotopic analyses. Mar. Micropaleontol. 107, 18–31. http://dx.doi.org/10.1016/j.marmicro.2013.12.004.

Dickens, G.R., 2000. Methane oxidation during the Late Palaeocene thermal maximum. Bull. Soc. Géol. Fr. 171, 37–49.

Dickens, G.R., 2011. Down the Rabbit Hole: toward appropriate discussion of methane release from gas hydrate systems during the Paleocene–Eocene thermal maximum and other past hyperthermal events. Clim. Past 7, 831–846.

Dickens, G.R., O'Neil, J.R., Rea, D.K., Owen, R.M., 1995. Dissociation of oceanic methane hydrate as a cause of the carbon isotope excursion at the end of the Paleocene. Paleoceanography 10, 965–971.

Dickens, G.R., Castillo, M.M., Walker, J.C.G., 1997. A blast of gas in the latest Paleocene: simulating first-order effects of massive dissociation of oceanic methane hydrate. Geology 25, 259–262.

Doney, S.C., Fabry, V.J., Feely, R.A., Kleypas, J.A., 2009. Ocean acidification: the other CO_2 problem. Annu. Rev. Mar. Sci. 1, 169–192. http://dx.doi.org/10.1146/annurev.marine.010908.163834.

Edgar, K.M., Bohaty, S.M., Gibbs, S.J., Sexton, P.F., Norris, R.D., Wilson, P.A., 2013. Symbiont 'bleaching' in planktic foraminifera during the Middle Eocene climatic optimum. Geology 41, 15–18.

Farley, K.A., Eltgroth, S.F., 2003. An alternative age model for the Paleocene–Eocene thermal maximum using extraterrestrial ^3He. Earth Planet. Sci. Lett. 208, 135–148.

Feely, R.A., Sabine, C.L., Lee, K., Berelson, W., Kleypas, J., Fabry, V.J., Millero, F.J., 2004. Impact of anthropogenic CO_2 on the $CaCO_3$ system in the oceans. Science 305, 362–366.

Foster, L.C., Schmidt, D.N., Thomas, E., Arndt, S., Ridgwell, A., 2013. Surviving rapid climate change in the deep sea during the Paleogene hyperthermals. Proc. Natl. Acad. Sci. USA 110, 9273–9276.

Gibbs, S.J., Bown, P.R., Sessa, J.A., Bralower, T.J., Wilson, P.A., 2006a. Nannoplankton extinction and origination across the Paleocene–Eocene thermal maximum. Science 314, 1770–1773.

Gibbs, S.J., Bralower, T.J., Bown, P.R., Zachos, J.C., Bybell, L.M., 2006b. Shelf-open ocean calcareous phytoplankton assemblages across the Paleocene–Eocene thermal maximum: implications for global productivity gradients. Geology 34, 233–236.

Gibbs, S.J., Stoll, H., Bown, P.R., Bralower, T.J., 2010. Ocean acidification and surface water carbonate production across the Paleocene–Eocene thermal maximum. Earth Planet. Sci. Lett. 295, 583–592.

Hancock, H.J., Dickens, G.R., 2006. Carbonate dissolution episodes in Paleocene and Eocene sediment, Shatsky Rise, west-central Pacific. In: Proceedings of the Ocean Drilling Program Scientific Results, vol. 198. Texas A&M University, pp. 1–24.

Haug, G.H., Tiedemann, R., 1998. Effect of the formation of the Isthmus of Panama on Atlantic Ocean thermohaline circulation. Nature 393, 673–676.

Hönisch, B., Ridgwell, A., Schmidt, D.N., Thomas, E., Gibbs, S.J., Sluijs, A., Zeebe, R., Kump, L., Martindale, R.C., Greene, S.E., Kiessling, W., Ries, J., Zachos, J.C., Royer, D., Barker, S., Foster, G.L., Williams, B., 2012. The geological record of ocean acidification. Science 335, 1058–1063.

Hovan, S.A., Rea, D.K., 1992. Paleocene–Eocene boundary changes in atmospheric and oceanic circulation: a southern hemisphere record. Geology 20, 15–18.

Howard, W.R., Prell, W.L., 1994. Late quaternary $CaCO_3$ production and preservation in the Southern Ocean: implications for oceanic and atmospheric carbon cycling. Paleoceanography 9 (3), 453–482.

Kaiho, K., Takeda, K., Petrizzo, M.R., Zachos, J.C., 2006. Anomalous shifts in tropical Pacific planktonic and benthic foraminiferal test size during the Paleocene–Eocene thermal maximum. Palaeogeogr. Palaeoclimatol. Palaeoecol. 237 (2), 456–464.

Kelly, D.C., 2002. Response of Antarctic (ODP Site 690) planktonic foraminifera to the Paleocene–Eocene thermal maximum: faunal evidence for ocean/climate change. Paleoceanography 17 (4), 23-1–23-13. http://dx.doi.org/10.1029/2002PA000761.

Kelly, D.C., Bralower, T.J., Zachos, J.C., Premoli Silva, I., Thomas, E., 1996. Rapid diversification of planktonic foraminifera in the tropical Pacific (ODP Site 865) during the late Paleocene thermal maximum. Geology 24, 423–426.

Kelly, D.C., Bralower, T.J., Zachos, J.C., 1998. Evolutionary consequences of the latest Paleocene thermal maximum for tropical planktonic foraminifera. Palaeogeogr. Palaeoclimatol. Palaeoecol. 141, 139–161.

Kelly, D.C., Zachos, J.C., Bralower, T.J., Schellenberg, S.A., 2005. Enhanced terrestrial weathering/runoff and surface ocean carbonate production during the recovery stages of the Paleocene–Eocene thermal maximum. Paleoceanography 20, PA4023. http://dx.doi.org/10.1029/2005PA001163.

Kelly, D.C., Nielsen, T.M.J., McCarren, H.K., Zachos, J.C., Röhl, U., 2010. Spatiotemporal patterns of carbonate sedimentation in the South Atlantic: implications for carbon cycling during the Paleocene–Eocene thermal maximum. Palaeogeogr. Palaeoclimatol. Palaeoecol. 293, 30–40.

Kelly, D.C., Nielsen, T.M.J., Schellenberg, S.A., 2012. Carbonate saturation dynamics during the Paleocene–Eocene thermal maximum: bathyal constraints from ODP Sites 689 and 690 in the Weddell Sea (South Atlantic). Mar. Geol.. http://dx.doi.org/10.1016/j.margeo.2012.02.003.

Kent, D.V., Cramer, B.S., Lanci, L., Wang, D., Wright, J.D., Van der Voo, R., 2003. A case for a comet impact trigger for the Paleocene/Eocene thermal maximum and carbon isotope excursion. Earth Planet. Sci. Lett. 211, 13–26.

Kirtland Turner, S., Ridgwell, A., 2013. Recovering the true size of an Eocene hyperthermal from the marine sedimentary record. Paleoceanography 28, 700–712. http://dx.doi.org/10.1002/2013PA002541.

Kleypas, J.A., Yates, K.K., 2009. Coral reefs and ocean acidification. Oceanography 22, 94–107.

Kozdon, R., Kelly, D.C., Kitajima, K., Strickland, A., Fournelle, J.H., Valley, J.W., 2013. In situ $\delta^{18}O$ and Mg/Ca analyses of diagenetic and planktic foraminiferal calcite preserved in a deep-sea record of the Paleocene–Eocene thermal maximum. Paleoceanography. http://dx.doi.org/10.1002/palo.20048.

Kranck, K., Smith, P.C., Milligan, T.G., 1996. Grain-size characteristics of fine-grained unflocculated sediments I: 'One-round' distributions. Sedimentology 43, 589–596.

Le, J., Shackleton, N.J., 1992. Carbonate dissolution fluctuations in the western equatorial Pacific during the late Quaternary. Paleoceanography 7 (1), 21–42.

Leon-Rodriguez, L., Dickens, G.R., 2010. Constraints on ocean acidification associated with rapid and massive carbon injections: the early Paleogene record at ocean drilling program site 1215, equatorial Pacific Ocean. Palaeogeogr. Palaeoclimatol. Palaeoecol. 298 (3), 409–420.

Lohbeck, K.T., Riebesell, U., Reusch, T.B.H., 2012. Adaptive evolution of a key phytoplankton species to ocean acidification. Nat. Geosci. 5, 346–351.

Lunt, D.J., Valdes, P., Dunkley, Jones T., Ridgwell, A., Haywood, A.M., Schmidt, D.N., Marsh, R., Maslin, M., 2010. CO_2-driven ocean circulation changes as an amplifier of Paleocene–Eocene thermal maximum hydrate destabilization. Geology 38, 875–878. http://dx.doi.org/10.1130/G31184.1.

McCarren, H., Thomas, E., Hasegawa, T., Röhl, U., Zachos, J.C., 2008. Depth dependency of the Paleocene–Eocene carbon isotope excursion: paired benthic and terrestrial biomarker records (Ocean Drilling Program Leg 208, Walvis Ridge). Geochem. Geophys. Geosyst. 9 (10). http://dx.doi.org/10.1029/2008GC002116.

McCave, I.N., Manighetti, B., Robinson, S.G., 1995. Sortable silt and fine sediment size/composition slicing: parameters for palaeocurrent speed and palaeoceanography. Paleoceanography 10, 593–610.

McCave, I.N., Hall, I.R., Bianchi, G.G., 2006. Laser versus settling velocity differences in silt grainsize measurements: estimation of palaeocurrent vigor. Sedimentology 53, 919–928. http://dx.doi.org/10.1111/j.1365-3091.2006.00783.x.

McInerney, F.A., Wing, S.L., 2011. The Paleocene–Eocene thermal maximum: a perturbation of carbon cycle, climate, and biosphere with implications for the future. Annu. Rev. Earth Planet. Sci. 39, 485.

Murphy, B.H., Farley, K.A., Zachos, J.C., 2010. An extraterrestrial (super 3) He-based time scale for the Paleocene–Eocene thermal maximum (PETM) from Walvis Ridge, IODP Site 1266. Geochim. Cosmochim. Acta 74, 5098–5108.

Nicolo, M.J., Dickens, G.R., Hollis, C.J., 2010. South Pacific intermediate water oxygen depletion at the onset of the Paleocene–Eocene thermal maximum as depicted in New Zealand margin sections. Paleoceanography 25, PA4210. http://dx.doi.org/10.1029/2009PA001904.

Norris, R.D., Kirtland Turner, S., Hull, P.M., Ridgwell, A., 2013. Marine ecosystem responses to cenozoic global change. Science 341, 492. http://dx.doi.org/10.1126/science.1240543.

Nunes, F., Norris, R.D., 2006. Abrupt reversal in ocean overturning during the Palaeocene/Eocene warm period. Nature 439, 60–63.

Orr, J.C., Fabry, V.J., Aumont, O., Bopp, L., Doney, S.C., Feely, R.A., Gnanadesikan, A., Gruber, N., Ishida, A., Joos, F., et al., 2005. Anthropogenic ocean acidification over the twenty-first century and its impact on calcifying organisms. Nature 437, 681–686.

Panchuk, 2007. Investigating the Paleocene/Eocene carbon cycle perturbation: an earth system model approach. Unpublished PhD thesis. The Pennsylvania State University. 70 pp.

Panchuk, K., Ridgwell, A., Kump, L.R., 2008. Sedimentary response to Paleocene–Eocene thermal maximum carbon release: a model-data comparison. Geology 36, 315–318.

Pandolfi, J.M., Connolly, S.R., Marshall, D.J., Cohen, A.L., 2011. Projecting coral reef futures under global warming and ocean acidification. Science 333, 418. http://dx.doi.org/10.1126/science.1204794.

Penman, D.E., Hönisch, B., Zeebe, R.E., Thomas, E., Zachos, J.C., 2014. Rapid and sustained surface ocean acidification during the Paleocene–Eocene Thermal Maximum. Paleoceanography 29 (5), 357–369. http://dx.doi.org/10.1002/2014PA002621.

Petrizzo, M.R., 2007. The onset of the Paleocene–Eocene thermal maximum (PETM) at Sites 1209 and 1210 (Shatsky Rise, Pacific Ocean) as recorded by planktonic foraminifera. Mar. Micropaleontol. http://dx.doi.org/10.1016/j.marmicro.2006.11.007.

Raffi, I., De Bernardi, B., 2008. Response of calcareous nannofossils to the Paleocene–Eocene thermal maximum: observations on composition, preservation and calcification in sediments from ODP Site 1263 (Walvis Ridge, SW Atlantic). Mar. Micropaleontol. 69, 119–138.

Raffi, I., Backman, J., Zachos, J.C., Sluijs, A., 2009. The response of calcareous nannfossil assemblages to the Paleocene Eocene thermal maximum at the Walvis Ridge in the South Atlantic. Mar. Micropaleontol. 70, 201–212. http://dx.doi.org/10.1016/j.marmicro.2008.12.005.

Ridgwell, A., 2007. Interpreting transient carbonate compensation depth changes by marine sediment core modeling. Paleoceanography 22, PA4102.

Ridgwell, A., Hargreaves, J.C., 2007. Regulation of atmospheric CO_2 by deep-sea sediments in an Earth system model. Glob. Biogeochem. Cycles 21, GB2008.

Ridgwell, A.T., Schmidt, D.N., 2010. Past constraints on the vulnerability of marine calcifiers to massive carbon dioxide release. Nat. Geosci. 3, 196–200. http://dx.doi.org/10.1038/ngeo75.

Robert, C., Kennett, J.P, 1994. Antarctic subtropical humid episode at the Paleocene–Eocene boundary: clay-mineral evidence. Geology 22, 211–214.

Röhl, U., Bralower, T.J., Norris, R.D., Wefer, G., 2000. A new chronology for the Late Paleocene thermal maximum and its environmental implications. Geology 28, 927–930.

Röhl, U., Westerhold, T., Bralower, T.J., Zachos, J.C., 2007. On the duration of the Paleocene–Eocene thermal maximum. Geochem. Geophys. Geosyst. 8. http://dx.doi.org/10.1029/2007GC001784.

Savrda, C.E., Bottjer, D.J., Gorsline, D.S., 1984. Development of a comprehensive oxygen-deficient marine biofacies model: evidence from Santa Monica, San Pedro, and Santa Barbara Basins, California Continental Borderland. In: AAPG Bulletin, vol. 68, pp. 1179–1192.

Schueth, J., Bralower, T.J., submitted for publication. The relationship between environmental change and the extinction of the nannoplankton Discoaster in the early Pleistocene. Paleoceanography.

Schlanger, S.O., Douglas, R.G., 1974. The pelagic ooze-chalk-limestone transition and its implications for marine stratigraphy. In: Hsu, K.J., Jenkyns, H.C. (Eds.), Pelagic Sediments: On Land and Under the Sea. In: Spec. Publ. Int. Assoc. Sedimentol., vol. 1, pp. 117–148.

Sluijs, A., Dickens, G.R., 2012. Assessing offsets between the $\delta^{13}C$ of sedimentary components and the global exogenic carbon pool across early Paleogene carbon cycle perturbations. Glob. Biogeochem. Cycles 26 (4). http://dx.doi.org/10.1029/2011GB004224.

Sluijs, A., Brinkhuis, H., Schouten, S., Bohaty, S.M., John, C., Zachos, J.C., Reichart, G.-J., Sinninghe Damsté, J.S., Crouch, E.M., Dickens, G.R., 2007a. Environmental precursors to rapid light carbon injection at the Paleocene/Eocene boundary. Nature 450, 1218–1221.

Sluijs, A., Bowen, G.J., Brinkhuis, H., Lourens, L.J., Thomas, E., 2007b. The Palaeocene–Eocene thermal maximum super greenhouse: biotic and geochemical signatures, age models and mechanisms of global change. In: Deep-Time Perspectives on Climate Change: Marrying the Signal from Computer Models and Biological Proxies. In: The Micropalaeontological Society, Special Publications. The Geological Society, London, pp. 323–349.

Stap, L., Sluijs, A., Thomas, E., Lourens, L., 2009. Patterns and magnitude of deep sea carbonate dissolution during Eocene thermal maximum 2 and H_2, Walvis Ridge, southeastern Atlantic Ocean. Paleoceanography 24, PA1211. http://dx.doi.org/10.1029/2008PA001655.

Stoll, H.M., 2005. Limited range of interspecific vital effects in coccolith stable isotopic records during the Paleocene–Eocene thermal maximum. Paleoceanography 20. http://dx.doi.org/10.1029/2004PA001046.

Stott, L.D., 1992. Higher temperatures and lower oceanic pCO_2: a climate enigma at the end of the Paleocene epoch. Paleoceanography 7, 395–404.

Stow, D.A.V., Faugeres, J.-C., Howe, J.A., Pudsey, C.J., Viana, A.R., 2002. Bottom currents, contourites and deep-sea sediment drifts: current state-of-the-art. Mem. Geol. Soc. Lond. 22, 7–20. http://dx.doi.org/10.1144/GSL.MEM.2002.022.01.02.

Takeda, K., Kaiho, K., 2007. Faunal turnovers in central Pacific benthic foraminifera during the Paleocene–Eocene thermal maximum. Palaeogeogr. Palaeoclimatol. Palaeoecol. 251 (2), 175–197.

Thomas, D.J., Zachos, J.C., Bralower, T.J., Thomas, E., Bohaty, S., 2002. Warming the fuel for the fire: evidence for the thermal dissociation of methane hydrate during the Paleocene–Eocene thermal maximum. Geology 30, 1067–1070.

Thomas, D.J., Bralower, T.J., Jones, C.E., 2003. Neodymium isotopic reconstruction of late Paleocene–early Eocene thermohaline circulation. Earth Planet. Sci. Lett. 209, 309–322.

Thomas, E., 1990. Late Cretaceous through Neogene deep-sea benthic foraminifers (Maud Rise, Weddell Sea, Antarctica). In: Proceedings ODP, Scientific Results, vol. 113, pp. 571–594.

Thomas, E., 1998. The biogeography of the late Paleocene benthic foraminiferal extinction. In: Aubry, M.-P., Lucas, S., Berggren, W.A. (Eds.), Late Paleocene–Early Eocene Biotic and Climatic Events in the Marine and Terrestrial Records. Columbia University Press, pp. 214–243.

Thomas, E., 2003. Extinction and food at the sea floor: a high-resolution benthic foraminiferal record across the Initial Eocene thermal maximum, Southern Ocean Site 690. In: Wing, S., Gingerich, P., Schmitz, B., Thomas, E. (Eds.), Causes and Consequences of Globally Warm Climates of the Paleogene. In: GSA Special Paper, vol. 369, pp. 319–332.

Thomas, E., 2007. Cenozoic mass extinctions in the deep sea: what perturbs the largest habitat on Earth? In: GSA Special Papers, vol. 424, p. 1.

Thomas, E., Shackleton, N.J., 1996. The Paleocene–Eocene benthic foraminiferal extinction and stable isotope anomalies. In: Knox, R.W.O'B., Corfield, R.M., Dunay, R.E. (Eds.), Correlation of the Early Paleogene in Northwest Europe. In: Geological Society Spec. Publ., vol. 101, pp. 401–441.

Thompson, J., Cook, G.T., Anderson, R., MacKenzie, A.B., Harkness, D.D., McCave, I.N., 1995. Radiocarbon age offsets in different-sized carbonate components of deep-sea sediments. Radiocarbon 37, 91–101.

Thunell, R.C., 1976. Optimal indices of calcium carbonate dissolution in deep-sea sediments. Geology 4, 525–528.

Walker, J.C.G., Kasting, J.F., 1992. Effects of fuel and forest conservation on future levels of atmospheric carbon dioxide. Palaeogeogr. Palaeoclimatol. Palaeoecol. 97, 151–189.

Westerhold, T., Röhl, U., Laskar, J., Raffi, I., Bowles, J., Lourens, L.J., Zachos, J.C., 2007. On the duration of magnetochrons C24r and C25n and the timing of early Eocene global warming events: implications from the Ocean Drilling Program Leg 208 Walvis Ridge depth transect. Paleoceanography 22. http://dx.doi.org/10.1029/2006PA001322.

Westerhold, T., Röhl, U., Raffi, I., Fornaciari, E., Monechi, S., Reale, V., Bowles, J., Evans, H.F., 2008. Astronomical calibration of the Paleocene time. Palaeogeogr. Palaeoclimatol. Palaeoecol. 257, 377–403.

Wing, S.L., Harrington, G.J., Smith, F.A., Bloch, J.I., Boyer, D.M., Freeman, K.H., 2005. Transient floral change and rapid global warming at the Paleocene–Eocene boundary. Science 310 (5750), 993–996.

Winguth, A.M., Thomas, E., Winguth, C., 2012. Global decline in ocean ventilation, oxygenation, and productivity during the Paleocene–Eocene thermal maximum: implications for the benthic extinction. Geology 40, 263–266.

Zachos, J.C., Pagani, M., Sloan, L., Thomas, E., Billups, K., 2001. Trends, rhythms, and aberrations in global climate 65 Ma to present. Science 292, 686–693.

Zachos, J.C., Wara, M.W., Bohaty, S., Delaney, M.L., Petrizzo, M.R, Brill, A., Bralower, T.J., Premoli-Silva, I., 2003. A transient rise in tropical sea surface temperature during the Paleocene–Eocene thermal maximum. Science 302, 1551–1554.

Zachos, J.C., Röhl, U., Schellenberg, S.A., Sluijs, A., Hodell, D.A., Kelly, D.C., Thomas, E., Nicolo, M., Raffi, I., Lourens, L.J., McCarren, H., Kroon, D., 2005. Rapid acidification of the Ocean during the Paleocene–Eocene thermal maximum. Science 308, 1611–1615.

Zachos, J.C., Bohaty, S.M., John, C.M., McCarron, H., Kelly, D.C., Nielson, T., 2007. The Palaeocene–Eocene carbon isotope excursion: constraints from individual shell planktonic foraminifer records. Philos. Trans. R. Soc. Lond. A 365, 1829–1842.

Zeebe, R.E., Zachos, J.C., 2007. Reversed deep-sea carbonate ion basin gradient during Paleocene–Eocene thermal maximum. Paleoceanography 22, PA3201. http://dx.doi.org/10.1029/2006PA001395.

Zeebe, R.E., Zachos, J.C., 2013. Long-term legacy of massive carbon input to the Earth system: Anthropocene versus Eocene. Philos. Trans. R. Soc. Lond. A 371, 20120006. http://dx.doi.org/10.1098/rsta.2012.0006.

Zeebe, R.E., Zachos, J.C., Dickens, G.R., 2009. Carbon dioxide forcing alone insufficient to explain Palaeocene–Eocene thermal maximum warming. Nat. Geosci. 2, 576–580.